6004 J. Org. Chem. 2001, 66, 6004−6013

# Lithium Reduction of the Bowl-Shaped $C_{60}$ Fragment Diindeno[1,2,3,4-*defg*;1′,2′,3′,4′-*mnop*]chrysene: An Interplay between Experiment and Calculation

Roy Shenhar,[†] Ronald Beust,[†] Roy E. Hoffman,[†] Itamar Willner,[†] Hindy E. Bronstein,[‡]
Lawrence T. Scott,[‡] and Mordecai Rabinovitz*,[†]

*Department of Organic Chemistry, The Hebrew University of Jerusalem, Jerusalem, Israel 91904, and*
*Department of Chemistry, Boston College, Chestnut Hill, Massachusetts 02467-3860*

*mordecai@vms.huji.ac.il*

*Received January 25, 2001*

Diindeno[1,2,3,4-*defg*;1′,2′,3′,4′-*mnop*]chrysene (DIC) (one of the smallest symmetrical bowl-shaped fragments of $C_{60}$) and its tetra-*tert*-butyl derivative are reduced with lithium metal to yield dianions and tetraanions. Due to the high degree of symmetry ($C_{2v}$) of DIC and its derivative, their NMR spectra cannot be assigned using the standard two-dimensional NMR techniques. A novel carbon-edited NOESY method was used to complete the assignments of the neutral and dianion species, whereas the tetraanions are aided by DFT calculations for their assignment. Experimental charge-distribution patterns were obtained and match those of the calculations. An extension of the empirical approach for estimating the charge distribution from the $^{13}C$ NMR spectra enables a direct comparison between experimentally derived charge-distribution data and the computed electron density in each of the lowest unoccupied molecular orbitals. The overall picture evolving from the orbital structure of DIC is presented and reflects the surface reactivity of $C_{60}$.

## Introduction

Planar, polycyclic, aromatic hydrocarbons (PAHs) exhibit unique chemical features that originate from their aromatic character since their electronic structure is a hybridization of several resonative configurations. Fullerenes, on the other hand, are ball-shaped PAHs that have, in addition, a strained topology, which affects the efficiency of the conjugation of the $\pi$-electrons and therefore influences their chemical properties.[1] Between these two extremes lies the family of concave PAHs, which exhibit properties of both families: similar to fullerenes, these bowl-shaped PAHs have curved surfaces, but unlike fullerenes, they also have a rim. Whereas the chemistry on their surfaces resembles that of fullerenes (e.g., addition reactions),[1,2] they may also undergo diverse chemical reactions on their rim,[2] similar to that of planar PAHs.

Concave PAHs, due to their highly strained topologies, only recently became available in quantities that permit investigation. The development of pyrolysis methods in the past decade paved the way for a new generation of PAHs to emerge. Small, concave fragments of fullerenes raise special interest since they might serve as model molecules for the different faces of fullerenes; understanding their nature will contribute to the understanding of the nature of fullerenes.

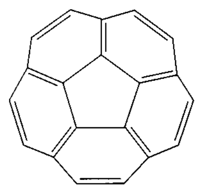

**1**

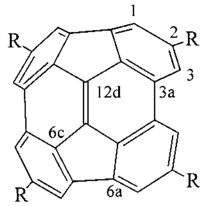

**2**

**2a** R=H
**2b** R=$^tBu$

Corannulene ($C_{20}H_{10}$, **1**) is the smallest highly symmetrical concave fragment of $C_{60}$, and it shows remarkable properties. Despite its small carbon skeleton it can be reduced with alkali metals to a reduction state as high as a tetraanion[3] via an antiaromatic intermediate (dianion) in the reduction process.[4] The lithium salt of the corannulene tetraanion was discovered to exist in the form of a dimer.[5] Also, corannulene facilitates the reduction of fullerenes under mild conditions, presumably by serving as an electron shuttle.[6]

Diindeno[1,2,3,4-*defg*;1′,2′,3′,4′-*mnop*]chrysene (DIC, $C_{26}H_{12}$, **2a**)[2,7] is another small, concave fragment of $C_{60}$. The central double bond at the hub of the bowl is exposed

---

* Corresponding author. Phone: ++972-2-6585281. Fax: ++972-2-6527547.

[†] The Hebrew University of Jerusalem.

[‡] Boston College.

(1) (a) Taylor, R.; Walton, D. R. M. *Nature* **1993**, *363*, 685−693. (b) Geckeler, K. E.; Samal, S. *Polym. Int.* **1999**, *48* (9), 743−757. (c) Hirsch, A. *Top. Curr. Chem.* **1999**, *199*, 1−65 and references therein. (d) Taylor, R. *Lecture Notes on Fullerene Chemistry: A Handbook for Chemists*; Imperial College Press: London, 1999.

(2) (a) Scott, L. T. *Pure Appl. Chem.* **1996**, *68*, 291−300. (b) Scott, L. T.; Bronstein, H. E.; Preda, D. V.; Ansems, R. B. M.; Bratcher, M. S.; Hagen, S. *Pure Appl. Chem.* **1999**, *71* (2), 209−219.

(3) Ayalon, A.; Rabinovitz, M.; Cheng, P.-C.; Scott, L. T. *Angew. Chem., Int. Ed. Engl.* **1992**, *31* (12), 1636−1637.

(4) Baumgarten, M.; Gherghel, L.; Wagner, M.; Weitz, A.; Rabinovitz, M.; Cheng, P.-C.; Scott, L. T. *J. Am. Chem. Soc.* **1995**, *117* (23), 6254−6257.

(5) (a) Ayalon, A.; Sygula, A.; Cheng, P.-C.; Rabinovitz, M.; Rabideau, P. W.; Scott, L. T. *Science* **1994**, *265*, 1065−1067. (b) Shabtai, E.; Hoffman, R. E.; Cheng, P.-C.; Bayrd, E.; Scott, L. T.; Rabinovitz, M. *J. Chem. Soc., Perkin Trans. 2* **2000**, 129−133.

(6) Shabtai, E.; Weitz, A.; Haddon, R. C.; Hoffman, R. E.; Rabinovitz, M.; Khong, A.; Cross, R. J.; Saunders, M.; Cheng, P.-C.; Scott, L. T. *J. Am. Chem. Soc.* **1998**, *120*, 6389−6393.

(7) (a) Hagen, S.; Nuechter, U.; Nuechter, M.; Zimmermann, G. *Tetrahedron Lett.* **1994**, *35*, 7013−7014. (b) Hagen, S.; Nuechter, U.; Nuechter, M.; Zimmermann, G. *Polycyclic Aromat. Compd.* **1995**, *4*, 209−217.

10.1021/jo010103f CCC: \$20.00

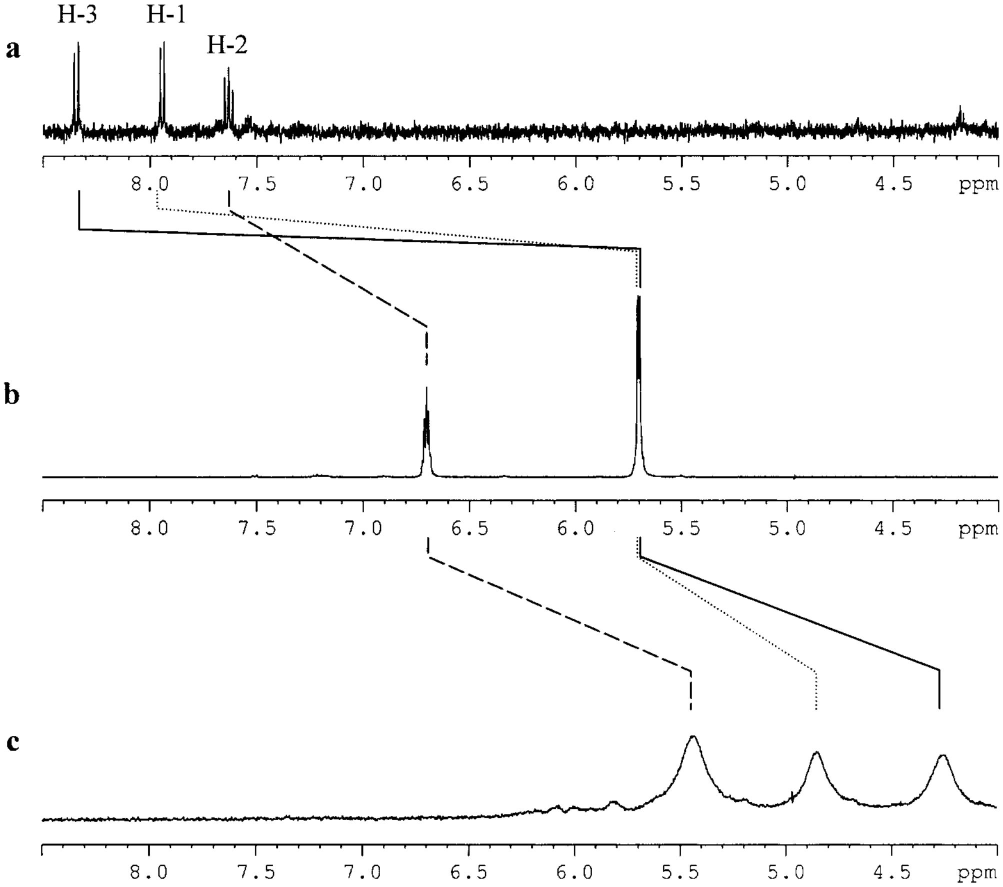

**Figure 1.** $^1$H NMR spectra recorded for the DIC (**2a**) in THF-$d_8$. (a) Neutral (298 K). (b) Dianion (230 K). (c) Tetraanion (165 K).

to nucleophilic attack,[2,8] similar to the double bonds in fullerenes. Thus, whereas corannulene is a fragment that exhibits the aromatic character of fullerenes, DIC serves as a fragment that demonstrates the surface reactivity of fullerenes.

Alkali metal reduction offers a relatively efficient way to investigate the electronic structure of PAHs. Insertion of additional electrons into the lowest unoccupied molecular orbitals (LUMOs) forms organic anions, which can be studied by spectroscopic methods (e.g., UV−vis, NMR, EPR, etc.). When the formation of the anion is not followed by a significant conformational change, the electronic structure of the anion may reveal the nature of the LUMO energy levels of the parent compound. This may aid in making predictions regarding the compound's properties.

The electronic structure of a PAH anion is usually revealed by calculating the charge distribution on the $\pi$-framework from the differences between the $^{13}$C NMR spectra of the anion and that of the neutral species, employing eq 1:

$$\rho = \Delta\delta/K_c \tag{1}$$

where $\rho$ is the charge density on the carbon atom, $\Delta\delta$ is the difference in the carbon atom's chemical shifts between the neutral species and the anion, and $K_c$ is a proportionality constant equal to the sum of differences in the chemical shifts for all the carbon atoms divided by the total charge.[9] The value of $K_c$, which is a molecular property, may give an indication of the total charge of the anion. Since $K_c$ is normalized with respect to the total charge, different $K_c$ values calculated for different reduction states should be comparable. Slight changes in $K_c$ values are often an indication of the paratropicity of the system, and it was suggested that we use an analogous equation for the protons (as the nuclei most influenced by anisotropic ring-current effects) to correct the proportionality constant of the carbons ($K_c$).[10] Nonetheless, when the aromatic character of a molecule is not changed drastically upon reduction, the local $\pi$-charge density is, indeed, the dominant factor influencing the individual $^{13}$C chemical shifts,[9] and the charge-distribution equation may be applicable with a reasonable accuracy without correction. Charge-distribution charts of anions obtained by this method serve as useful guides to chemical intuition by pointing to molecular sites where the charge is concentrated or absent, thereby implying the type of chemistry the molecule might exhibit.

A nonexperimental but more direct way to study the closest LUMOs of a PAH is quantum mechanical calculations. The development of DFT methods made reliable and time-efficient calculations on medium-size PAHs and their anions feasible.[11] Along with the explicit structure of the orbitals, DFT calculations also yield important conformational predictions. Nevertheless, since calculat-

---

[8] Bronstein, H. E.; Scott, L. T. Quoted in Baum, R. *Chem. Eng. News* **1997**, *75* (48), 28.

[9] (a) Müllen, K. *Chem. Rev.* **1984**, *84*, 603−646 and references therein. (b) Rabinovitz, M. *Top. Curr. Chem.* **1988**, *146*, 99−169 and references therein.

[10] (a) Eliasson, B.; Edlund, U.; Müllen, K. *J. Chem. Soc., Perkin Trans. 2* **1986**, 937−940. (b) Eliasson, B.; Johnels, D.; Sethson, I.; Edlund, U.; Müllen, K. *J. Chem. Soc., Perkin Trans. 2* **1990**, 897−900.

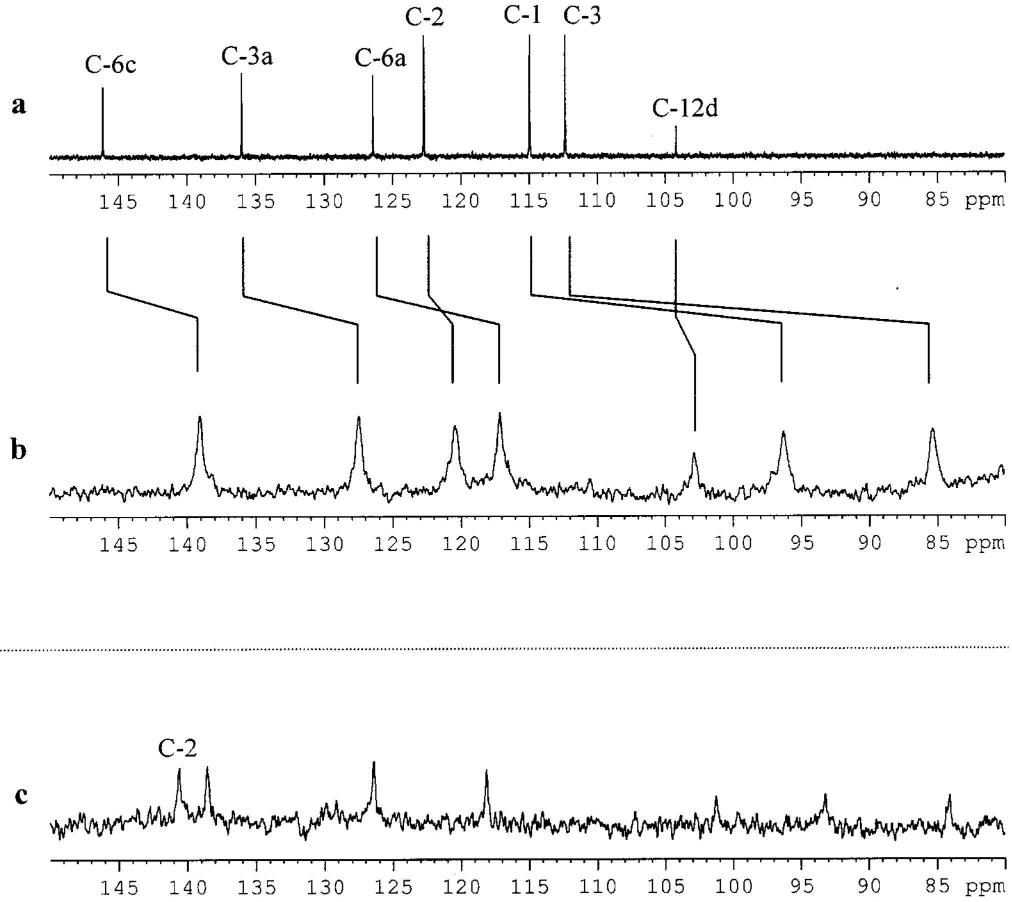

**Figure 2.** $^{13}$C NMR spectra recorded in THF-$d_8$. (a) **2a** dianion (230 K). (b) **2a** tetraanion (165 K). (c) **2b** tetraanion (165 K). Note that C-12d always corresponds to the weakest peak in the spectrum, and also the identification of the C-2 peak in the tetraanions as the only peak appearing at significantly different fields in **2a**$^{4-}$ and **2b**$^{4-}$.

ing anions of medium-size PAHs is still at the boundary of the calculation ability, a comparison between data predicted from calculation and those obtained from experiment is most desirable and important.

Herein we wish to report on our theoretical and experimental study on the lithium reduction of DIC (**2a**) and its derivative **2b**, which yield di- and tetraanions.

## Results and Discussion

The DIC system was studied both experimentally and theoretically. All structures referred to hereafter were geometrically optimized within their symmetry groups and found to be minimum-energy structures (or saddle points of the first order for transition-state structures). See Experimental Section for details.

**Neutral Compounds 2a and 2b.** To calculate the charge distribution from the $^{13}$C NMR spectra, a complete assignment of the spectra must be obtained. This is usually done with a combination of two-dimensional NMR experiments. Through-bond couplings (employing COSY) and through-space interactions (revealed in a NOESY experiment) between protons are usually sufficient to fully assign the $^{1}$H NMR spectrum. The $^{13}$C NMR spectrum is then assigned by using a combination of a single-bond $^{13}$C$-$$^{1}$H correlation experiment and a heteronuclear multiple-bond correlation (HMBC) experiment, which shows $^{13}$C$-$$^{1}$H correlations over three bonds. In cases when the $^{1}$H NMR spectrum cannot be completely assigned by COSY and NOESY, the redundancy of information obtained from the HMBC experiment usually resolves both the $^{1}$H NMR and the $^{13}$C NMR spectra (e.g., for perylene).

A close inspection of the carbon skeleton of DIC (**2a**) reveals an interesting phenomenon with respect to the ability to assign its $^{1}$H NMR and $^{13}$C NMR spectra (Figures 1 and 2). Standard two-dimensional methods can resolve neither the dichotomy between positions 1 and 3 (both in carbons and in protons) nor that between C-3a and C-6a. To assign H-1 and H-3 in the neutral compound, assumptions must be made regarding the influence of the overcrowding in the different bay regions on the chemical shifts. Unfortunately, even these assumptions are worthless when trying to assign the spectra of the charged species. Charge effects as well as paratropic ring currents, which may occur when the number of electrons is increased by two, may in principle affect the chemical shifts more than the proton overcrowding, resulting in a reversed order of the peaks.

A downfield chemical shift effect is actually only a secondary indication of bay-proton overcrowding. First and foremost, this situation expresses itself by a strong correlation in the NOESY spectrum between the two

---

(11) (a) Parr, R. G.; Yang, W. *Density-Functional Theory of Atoms and Molecules*; Oxford University Press: Oxford, 1989. (b) Ziegler, T. *Chem. Rev.* **1991**, *91*, 651$-$667. (c) Laird, B. B., Ross, R. B., Ziegler, T., Eds. *Chemical Applications of Density Functional Theory*; ACS Symposium Series 629; American Chemical Society: Washington, DC, 1996. (d) Kohn, W.; Becke, A. D.; Parr, R. G. *J. Phys. Chem.* **1996**, *100*, 12974$-$12980.

**Table 1. Calculated (GIAO/B3LYP/6-311G**//B3LYP/6-311G**) vs Experimental Chemical Shifts (ppm) for DIC (2a)**

| atom no. | neutral | | dianion | | tetraanion | |
|---|---|---|---|---|---|---|
| | exp. | calcd | exp. | calcd | exp. | calcd |
| C-1 | **123.16** | 127.99 | **114.95** | 124.85 | **96.6** | 99.41 |
| C-2 | **129.62** | 134.24 | **122.70** | 114.62 | **120.7** | 118.73 |
| C-3 | **125.21** | 129.95 | **112.34** | 114.72 | **85.6** | 88.31 |
| C-3a | **134.15** | 139.70 | **136.01** | 144.79 | **127.7** | 135.94 |
| C-6c | **139.32** | 144.71 | **146.06** | 152.67 | **139.3** | 144.72 |
| C-6a | **142.38** | 148.89 | **126.43** | 130.58 | **117.4** | 123.12 |
| C-12d | **137.31** | 141.40 | **104.17** | 116.78 | **103.1** | 111.17 |
| $^{13}$C CM[a] | **132.69** | 137.87 | **124.70** | 129.33 | **113.7** | 117.82 |
| **$^{13}$C Corr.**[b] | | **99.6%** | | **89.6%** | | **98.4%** |
| H-1 | **7.96** | 8.07 | **5.7** | 6.53 | **4.89** | 3.54 |
| H-2 | **7.69** | 7.81 | **6.7** | 5.38 | **5.46** | 4.64 |
| H-3 | **8.30** | 8.45 | **5.7** | 5.63 | **4.28** | 3.62 |

[a] $^{13}$C NMR spectrum center-of-mass (weighted average). [b] Correlation coefficient between the calculated and experimental sets of values (calculated only for $^{13}$C NMR values).

overcrowded protons. A stronger NOE peak between protons in a narrower bay would remain a valid distinction tool between the two types of bays, even when ring-current effects blur the downfield chemical-shift effect. The recent development of a two-dimensional carbon-edited NOESY experiment, which takes advantage of the natural isotopic substitution of $^{12}$C with $^{13}$C in symmetrical bay regions to break the symmetry and detect useful NOE correlations across these regularly symmetrical bays, enabled the unequivocal assignment of the $^{1}$H NMR spectrum of DIC (**2a**) through the assignment of 2,5,8,11-tetra-*tert*-butyldiindeno[1,2,3,4-*defg*;1′,2′,3′,4′-*mnop*]chrysene (**2b**).[12] This tetrasubstituted derivative of DIC reveals the same assignment problems, yet it is substantially more soluble than the parent compound in all solvents. Since the $^{13}$C NMR and $^{1}$H NMR spectra of both DIC (**2a**) and its derivative **2b** are comparable (besides at C-2, which is shifted to a low field in **2b** because of the substitution), the complete assignment of DIC (**2a**) could be deduced from the complete assignment of **2b**.

DFT calculations correlate well with the experimental values and confirm the assignment (Table 1, see also Experimental Section).

**Dianions.** Reacting DIC (**2a**) with lithium metal results in a change in the color of the solution, from pale yellow to dark red, along with the disappearance of the NMR spectra. This is attributed to the conversion of the neutral molecule to its radical anion (**2a**$^{\bullet-}$). Further reduction changes the color of the solution to brown, and new $^{1}$H NMR and $^{13}$C NMR spectra evolve (Figures 1 and 2). These spectra are attributed to the dianion (**2a**$^{2-}$), and the $^{1}$H NMR spectrum exhibits another assignment difficulty: the absorption peaks corresponding to protons H-1 and H-3 are accidentally overlapping and are inseparable even at a wide range of temperatures. Therefore, the carbon-edited NOESY experiment could not be applied. Fortunately, the dianion of **2b** offered a solution. Apparently, the *tert*-butyl substitution at position 2 influences protons H-1 and H-3 in **2b**$^{2-}$ so that their $^{1}$H NMR bands are separated by almost 1 ppm. The $^{13}$C NMR spectrum of **2b**$^{2-}$ (not shown) is still similar to that of **2a**$^{2-}$ (besides at C-2 as before), and thus, the method of assigning the spectra of DIC (**2a**) on the basis of the assignment of **2b** using the carbon-edited NOESY method could be applied to the respective dianions.

The carbon-edited NOESY spectrum of **2b**$^{2-}$ is a bit surprising since it reveals the more crowded proton H-3 (always showing the strongest carbon-edited NOE correlation) as the *less deshielded* proton of the two aromatic protons. This phenomenon is consistent over a wide range of mixing-time delays which were applied to the carbon-edited NOESY pulse sequence to avoid erring due to differences in the relaxation times of the two protons. Calculations of **2a**$^{2-}$ reproduce the same trend for both $^{13}$C NMR and $^{1}$H NMR spectra (Table 1), along with the supporting conclusion that the interproton distance across the "phenanthrene-type" bay is shorter than that across the "fluorene-type" bay, even in the dianion. The last confirmation is important to validate the assumption that serves as the basis for the assignment of the $^{1}$H NMR peaks using the carbon-edited NOESY spectrum. Applying the standard heteronuclear two-dimensional NMR methods, we completed the assignment for the carbons of the dianions **2a**$^{2-}$ and **2b**$^{2-}$.

The $^{7}$Li NMR spectrum shows a single absorption band at ca. 0 ppm, indicating a strong solvation of the cations by the THF molecules. This is expected when a large anion (with $\pi$-charge delocalization) and small cations in a polar solvent are involved.[9] Therefore, it seems that in the calculations, one could neglect the cations along with the solvent molecules in order to simulate correctly the solvation state of the anionic salt. To test this assumption, we calculated **2a**$^{2-}\cdot 2\mathrm{Li}^{+}$ with all possible arrangements of two lithium cations, and as expected, the computed NMR chemical shifts agree less (less than 85% correlation) with the experimental values than with those computed for the bare **2a**$^{2-}$ (Table 1). Therefore, the bare dianion is taken as the best gas-phase model for the dianionic salt in solution.

**Tetraanions.** Further contact of the **2a**$^{2-}$ solution with the lithium wire leads to a second disappearance of the NMR spectrum (attributed to **2a**$^{\bullet 3-}$). This is accompanied by a gradual change of the color to dark green, and then to the evolution of a new $^{1}$H NMR spectrum (Figure 1), which is attributed to **2a**$^{4-}$. Although the $^{1}$H NMR spectrum is weak and fairly broad (typical bandwidth >20 Hz), we could still record the $^{13}$C NMR spectrum of the tetraanions (Figure 2).

The characteristics of the one-dimensional NMR spectra preclude the possibility of obtaining any long-range proton−carbon correlations using an HMBC experiment. Only partial assignment could be deduced experimentally. As in the case of the neutral and dianion species, C-2 is assigned in both species to the only carbon band showing a substantially different chemical shift between **2a**$^{4-}$ and **2b**$^{4-}$. The short-range $^{13}$C−$^{1}$H correlation spectrum of **2b**$^{4-}$ distinguishes C-1 and C-3 from the remaining six aromatic carbon bands, yet does so without any way to resolve between C-1 and C-3. Furthermore, the weakest peak in both $^{13}$C NMR spectra is assigned to C-12d since it is at least four bonds away from any proton. As is known, the proton decoupling performed during acquisition of the $^{13}$C NMR spectrum usually results in the enhancement of the absorption peaks of carbon atoms that are close to protons through NOE effects.[13] This phenomenon is also observed in the spectra of the dianion and the neutral species, as the bands of C-12d are always the weakest in intensities.

---

(12) Hoffman, R. E.; Shenhar, R.; Willner, I.; Bronstein, H. E.; Scott, L. T.; Rajca, A.; Rabinovitz, M. *Magn. Reson. Chem.* **2000**, *38*, 311−314.

Considering the difficulty of obtaining any further experimental data, we used DFT calculations to complete the assignment. Although **2a**$^{4-}$ is a highly charged species, we find that the computed NMR chemical shifts are in excellent agreement with the experimental values (Table 1). In particular, we find that the calculation's assignment is in accordance with our partial experimental assignment for the peaks of C-1/C-3, C-2, and C-12d, resolving the ambiguity between C-1 and C-3 along with completing the assignment for C-3a, C-6a, and C-6c. Consistent with the trend observed in the dianion, it is found that H-1 is more deshielded than H-3 in the tetraanion as well, although the former is less overcrowded than the latter.

Contrary to that of the dianion, the $^7$Li NMR spectra of **2a**$^{4-}$ and **2b**$^{4-}$ show several absorption bands ranging from +2 to −7 ppm. These types of high-field $^7$Li NMR chemical shifts usually indicate a strong coordination between the cations and the organic framework. As the extra charge in **2a**$^{4-}$ is rather delocalized over the whole $\pi$-framework, it is somewhat less plausible to assume that the affinity of the charged carbon framework for the cations would be greater than the affinity of the solvent molecules for the cations.[9] Calculating all possible arrangements of **2a**$^{4-}\cdot 4Li^+$ indeed shows that the computed NMR chemical shifts agree less with the experimental values (less than 70% correlation for the lowest-energy structures) than the values computed for the bare tetraanion (Table 1), similar to our findings for the dianion. These calculations merely reveal the tip of the iceberg of the solvation effect; therefore, we cannot rule out the possibility of different solvation modes of some of the lithium cations with different degrees of association with the polycyclic anion. However, calculating all the possible combinations of lithium cations with the organic anion (with or without the inclusion of solvent molecules) is beyond the scope of this paper. Yet, another situation that might afford an explanation both to the high-field chemical-shift effect and to the multiple peaks observed in the $^7$Li NMR spectrum is that of stacked aggregation modes, e.g., a dimer, in which the lithium cations serve as an electrostatic glue that attracts the charged decks together. This is the situation in the tetraanion derived from corannulene (**1**$^{4-}$) with lithium, which is known to exist as a dimer in solution.[5] In such systems, the lithium cations are sandwiched between two negatively charged aromatic decks and are thus strongly shielded by ring currents. A dimer, for example, is expected to interchange between various conformations, thus yielding broad peaks in the $^1$H NMR spectrum as observed. DFT calculations (B3LYP/6-31G*) performed on various arrangements of $(DIC^{4-})_2\cdot 4Li^+$ (out of the possible 12 arrangements of $DIC^{4-}/4Li^+/DIC^{4-}$) resulted in several low-energy arrangements, with almost perfect correlation between their NMR chemical shift values and their experimental values (a slight improvement compared to the bare **2a**$^{4-}$ values calculated with the same method and basis set). Indeed, the energy differences between these arrangements are small (less than 3.5 kcal/mol); therefore, the arrangements are predicted to interchange in the NMR time scale to yield an averaged, broad spectral pattern. However, since no firm experimental evidence for dimerization exists, the possibility of aggregation is merely proposed as a suggestion.

Quenching the tetraanionic solutions of both **2a**$^{4-}$ and **2b**$^{4-}$ with oxygen quantitatively yields the respective neutral hydrocarbons.

**Charge-Distribution and MO Analyses.** The complete assignment of the $^{13}$C NMR spectra of all the species enabled us to perform a charge-distribution analysis. The $K_c$ values calculated for **2a**$^{2-}$ and **2a**$^{4-}$ are 104.7 and 124.1 ppm/$e^-$, respectively. The center-of-mass of the $^{13}$C NMR spectra shifts upfield by 8.1 ppm upon the transformation of the neutral system into the dianion and by an additional 11.0 ppm when the latter is converted into the tetraanion. The $K_c$ values are similar and so are the shifts of the center-of-mass of the $^{13}$C NMR spectra, thus supporting the identification of the second diamagnetic charged species as the tetraanion of DIC.

Comparisons between the experimental results and the DFT calculations are performed using NMR chemical shift values, charge distribution (experimental vs NBO[14] analysis), and a qualitative comparison between the experimental charge distribution and the atomic orbital (AO) coefficients of the relevant frontier orbitals.

The comparison between the experimental chemical shifts and the computed isotropy shows a good correlation and assisted in completing the assignment of both $^1$H NMR and $^{13}$C NMR spectra as described in the previous sections.

Figure 3 shows the comparison between the charge-distribution values calculated from the $^{13}$C NMR spectra and the values computed using NBO analysis on the optimized structures for both **2a**$^{2-}$ and **2a**$^{4-}$. The correlation coefficient between these two series of values is higher than 70%. As both methods of evaluation of the charge distribution are mere approximations (the experimental method neglects paratropicity effects, and the DFT calculations neglect solvation and ion-pairing equilibria), the derived correlation represents a relatively good agreement between the experimental and computed results. Moreover, the known tendency of quantum MO calculations to indicate a more uniform charge distribution[15] is also reproduced here.

Comparing experimental charge-distribution results with the electronic structure, as depicted by the AO coefficients of the relevant frontier orbital, is not trivial since charge density is not an observable quality that can be derived from the wave function. Whereas *electron* density has probability meaning, *charge* density represents a somewhat vague measure, which is basically intended to help developing chemical intuition. Whereas *electron* density in a certain orbital is calculated directly from its AO coefficients (taking into account the overlap between each couple of AOs), *charge* density involves *all* orbitals in its estimation, therefore complicating the way the overlap elements are to be considered. In the approximation involved in featuring the charge density, one has to apply a certain degree of arbitrariness to the way in which the electron density between two atoms is divided. Nevertheless, when the charging process does not result in a substantial conformational change (as is the case in PAHs that are composed of fused rings, having limited conformational freedom), the structure of

---

[13] Solomon, I. *Phys. Rev.* **1955**, *99* (2), 559−565.

[14] (a) Foster, J. P.; Weinhold, F. *J. Am. Chem. Soc.* **1980**, *102*, 7211−7218. (b) Reed, A. E.; Weinhold, F. *J. Chem. Phys.* **1983**, *78*, 4066−4073. (c) Reed, A. E.; Weinhold, F. *J. Chem. Phys.* **1985**, *83*, 1736−1740.

[15] Müllen, K.; Huber, W.; Meul, T.; Nakagawa, M.; Iyoda, M. *J. Am. Chem. Soc.* **1982**, *104*, 5403−5411.

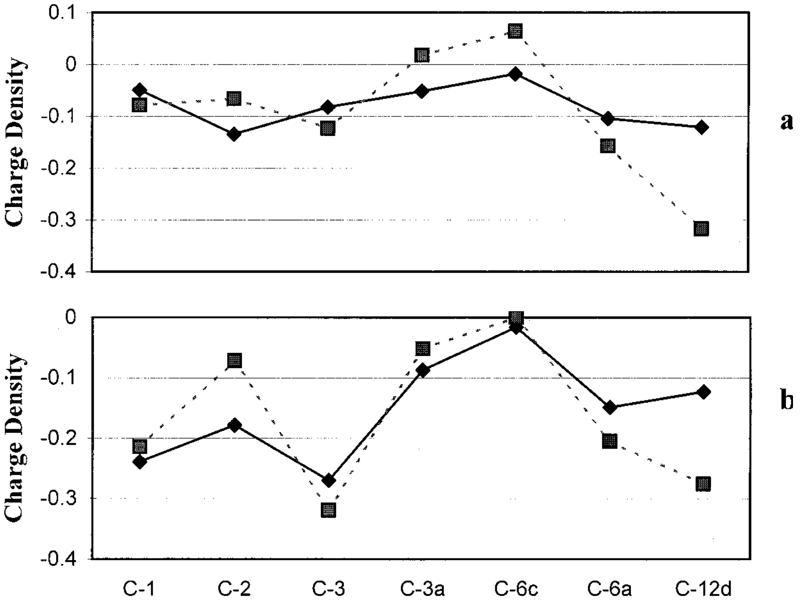

**Figure 3.** Experimental (from $^{13}$C NMR spectra, dashed line) vs computed (from NBO analysis, solid line) charge distributions calculated for DIC (**2a**). (a) Dianion. (b) Tetraanion.

the orbitals does not usually change significantly due to the change in the electron population. In other words, the HOMO of the dianion and the HOMO of the tetraanion would be almost identical to the LUMO and LUMO+1 of the neutral compound, respectively, as is indeed found for the orbitals of **2a**. Moreover, if the LUMO orbitals are not too dense (as is the case in small molecules of low symmetry), then the electronic state of a closed-shell anion would be described reliably by a single determinant, with no need for configuration interaction (which involves a mixing of the LUMO orbitals).[10b] This is indeed the case in **2a**, as the computed energy difference between the three closest LUMOs is at least 10 kcal/mol. Consequently, insertion of two additional electrons into the neutral **2a** would result in a charge-distribution chart that should resemble the *electron density* picture of the LUMO of **2a** (given that the aromatic character of the charged species is not changed much due to the reduction). The same applies for the analysis of the charge distribution of the tetraanion versus the LUMO+1 of the neutral system; here, however, one should be able to isolate the contributions to the charge distribution made solely by the LUMO+1 orbital. Our approach is to subtract the tetraanion's chemical shifts from those of the *dianion* (instead of from those of the neutral system) in the charge-distribution equation, regarding the tetraanion as a *dianion* of the dianion (i.e., assigning a total charge of 2− instead of 4− in the calculation of $K_c$). We will refer to the result of this type of calculation as the *referenced* charge distribution.

Figure 4 shows the total and referenced charge-distribution charts of the reduced species of **2a** along with the orbital structure of the closest HOMO and LUMO orbitals obtained from DFT calculations (employing the 6-31G* basis set) that were performed on the neutral compound. A qualitative comparison between the referenced charge-distribution charts of $\mathbf{2a}^{2-}$ and $\mathbf{2a}^{4-}$ and the squared AO coefficients of the LUMO orbitals (representing the electron density in these orbitals) shows a good agreement between them. The main features that should be mentioned include (a) a high electron (and charge) density on the central double bond in the dianion, reflecting the known tendency of neutral DIC to undergo nucleophilic addition reactions at this double bond;[2,8] (b) the lack of additional electron density on the central double bond (as well as on C-2) in the tetraanion, as predicted from the referenced charge-distribution analysis; and (c) the resemblance of the frontier orbitals of DIC to those of $C_{60}$ (as depicted in ref 1c).

An important conclusion is that under the restrictions discussed above, predictions about the electronic structure of the closest LUMO orbitals of a PAH can be made *experimentally*. If a molecule complies to certain constraints, then by reducing it and performing a referenced charge-distribution analysis (i.e., referring the $^{13}$C NMR chemical shift values of each reduction state to the *former* diamagnetic reduction state), one can obtain a good approximation to the electron density of the respective LUMO orbitals.

Further comparison of the orbital structure of a molecule to those of known building blocks can contribute significantly to the construction of a model describing the electronic nature of the molecule. For this purpose, we computed the canonical orbitals of benzene using the same geometrical parameters. Near each of the four DIC orbitals depicted in Figure 4 we placed the corresponding canonical benzene orbital. This comparison reveals that DIC is basically constructed of four benzene rings attached to a central double bond. The HOMO−1 shows a mixing of four of the same type ($\Psi_2$) of low-lying benzene orbitals in an antibonding fashion, with no mixing with the central double bond. In the HOMO, the same $\Psi_2$-benzene orbitals are present (this time in a bonding fashion) along with the known bonding orbital of a double bond. Antibonding interaction between the benzene moieties and the double bond causes a slight elevation of the energy of the HOMO in comparison to that of the HOMO−1 (2.6 kcal/mol). The mixing of both the double bond and the benzene moieties causes a slight distortion of the benzene fragment orbitals, which does not affect their phase pattern. The high energy of the LUMO (88.2 kcal/mol compared to the energy of the HOMO) is caused by the antibonding orbital of the double-bond fragment,

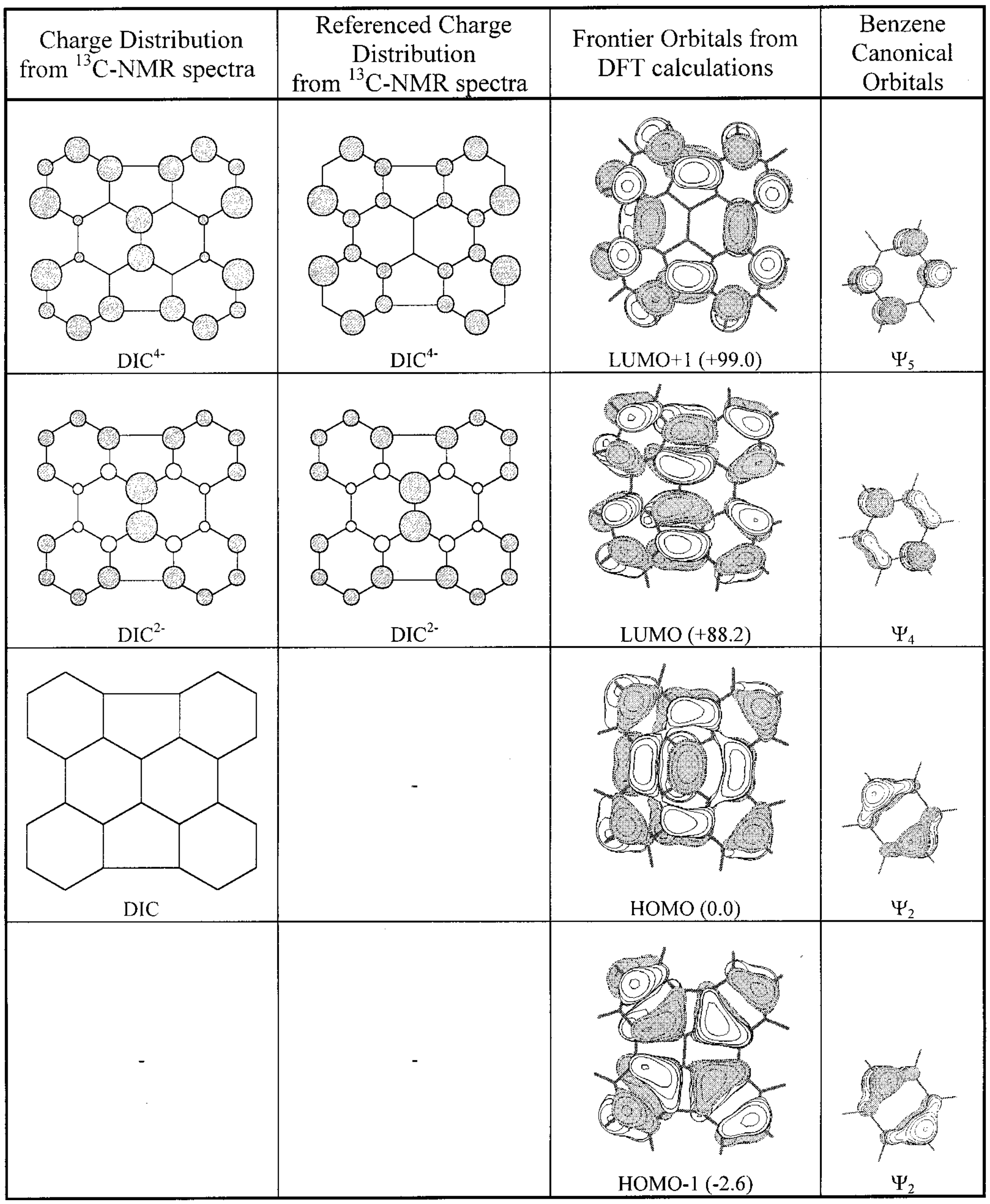

**Figure 4.** Charge-distribution charts calculated from the $^{13}$C NMR spectra of the reduced species of DIC (**2a**), and orbital coefficients calculated for the neutral **2a** and benzene using the DFT (B3LYP/6-31G*) level. Relative energies (kcal/mol) are given in parentheses. The first column shows charge-distribution charts calculated for each reduction state of **2a** by referring its $^{13}$C NMR spectrum to the spectrum of the neutral **2a**. The second column shows charge-distribution charts calculated for each reduction state of **2a** by referring its $^{13}$C NMR spectrum to the spectrum of the former diamagnetic reduction state.

which is further mixed with benzene orbitals of an antibonding type ($\Psi_4$). Similar to the HOMO, a coefficient distortion is imposed on the benzene orbitals (especially in C-1-type positions that do not retain the original phase) by a mixing of the moieties of both types. In the LUMO+1, four orbitals of another antibonding-type benzene orbital ($\Psi_5$) are mixed in a bonding fashion. Clearly, the orbitals composed of only benzene-type orbitals (namely, the HOMO−1 and LUMO+1) show remarkable resemblance to their corresponding canonical benzene orbitals.

The frontier orbital structure may give an explanation for the inverted order of bands between positions 1 and 3 in the dianions and tetraanions of **2a** and **2b**, as mentioned in the previous sections. Since the HOMO exhibits similar values of the coefficients at positions 1 and 3, the order between their absorption peaks in neutral DIC is dictated by the overcrowding effect, rendering H-3 as the more deshielded proton. As the absolute value of the AO coefficient for position 1 is significantly smaller than that for position 3 in the LUMO of **2a** (the dianion's frontier orbital), position 3 should be more shielded by electron density than position 1 in the dianion. Whereas the charge shielding and the overcrowding effect compensate each other in the $^{1}$H NMR spectrum of **2a**$^{2-}$, the charge effect in **2b**$^{2-}$ is the dominant factor, resulting in an inverted order of the proton peaks. Since carbon atoms are less affected by the bay-proton overcrowding, the inverted order of the $^{13}$C NMR peaks is observable in both **2a**$^{2-}$ and **2b**$^{2-}$. The electron density pattern in the LUMO+1 of **2a** (the tetraanion's frontier orbital) does not change the charge-

**Table 2. Bowl Depths and Bowl-to-Bowl Inversion Energy Barriers Calculated for the Different Reduction States of DIC (2a)**

| charging state | | HF/ 3-21G | HF/ 6-311G** | B3LYP/ 6-31G* | B3LYP/ 6-311G** | *m*PW1PW/ 6-311G** |
|---|---|---|---|---|---|---|
| neutral | *a* | 1.352 | 1.253 | 1.303 | 1.355 | 1.355 |
| | *b* | **6.95** | **5.57** | **5.24**[16] | **6.69**[16] | **6.80** |
| dianion | *a* | 1.453 | 1.398 | 1.390 | 1.449 | 1.453 |
| | *b* | **11.85** | **11.00** | **8.76** | **10.95** | **11.36** |
| tetraanion | *a* | 1.245 | 1.296 | 1.168 | 1.309 | 1.308 |
| | *b* | **5.68** | **7.25** | **3.77** | **6.53**[17] | **6.65** |

[a] Bowl depth (Å) was taken as the perpendicular distance between C-12d and C-2. [b] Inversion barrier (kcal/mol).

shielding trend between the two positions as it exhibits similar absolute values of the AO coefficients on both positions 1 and 3. Therefore, in the tetraanion, the same order of peaks existing in the dianion is retained, and the difference between them is rather enhanced.

A principal power of quantum calculations is the ability to predict conformational features of the molecules. In the context of the charged species of DIC, the most interesting geometrical parameter is the bowl depth. Table 2 shows the bowl depth along with the energy barrier for bowl-to-bowl inversion[16] calculated for each reduction state. The barriers are calculated from the energy difference between the minimum-energy bowl-shaped structure ($C_{2v}$) and the corresponding planar (or slightly twisted from planarity) structure. The planar ($D_{2h}$) structures were found to be saddle points of the first order in all reduction states with all methods of calculation except for DIC$^{4-}$ at the B3LYP/6-311G** level, for which its transition state is a slightly twisted $D_2$ structure.[17] The results[18] show a clear correlation between the bowl depth and the bowl-to-bowl inversion barrier.[19] It is found that the bowl becomes deeper when DIC is transformed into its dianion and becomes shallow again upon reduction to the tetraanion. This can be rationalized from the structure of the frontier orbital in each case. The LUMO of **2a** (the dianion's frontier orbital) exhibits a strong antibonding interaction of the central double-bond fragment orbital, causing a strong electronic repulsion between the two fluorene-type fragments of DIC at the hub of the bowl, thus making the bowl deeper. Antibonding interactions at the rim in the phenanthrene-type bay regions reinforce this effect. In the LUMO+1 of **2a** (the tetraanion's frontier orbital), there is a node on the central double bond; therefore, the charge of the last two electrons is distributed on the rim. Flattening and widening the bowl (like an opening flower) would make the perimeter larger, thus allowing for a better spatial distribution of the mutually repulsing extra electrons.

The last observation also supports the suggestion made previously regarding aggregation of the tetraanion: as the compound's skeleton approaches planarity again, and the energy barrier for the bowl-to-bowl inversion decreases upon reduction to the tetraanion, the overall shape of this tetraanion resembles a plate (in average) rather than a bowl. Thus, the two faces of the tetraanion become more similar (as opposed to distinct convex/concave faces as in the dianion), increasing the odds of forming a stacked aggregate upon collision. Moreover, the relative flexibility calculated for the tetraanionic decks further supports the assumption that an aggregate consisting of such decks would rapidly interchange between different arrangements, thus exhibiting broad lines in the NMR spectra and several $^7$Li NMR peaks, as was indeed observed.

## Conclusions

DIC (**2a**) and its tetra-*tert*-butyl derivative (**2b**) were reduced with lithium, affording dianions and tetraanions. Whereas the assignment of the NMR spectra of the neutral compounds and their dianions **2a**$^{2-}$ and **2b**$^{2-}$ could be achieved unambiguously by direct experimental means, the spectra of the tetraanions **2a**$^{4-}$ and **2b**$^{4-}$ could only be partially assigned experimentally and had to be assisted by computation. Good correlation between the experimental charge distribution (obtained from the change in the $^{13}$C NMR chemical shifts) and the computed charge distribution was obtained. A direct correlation could be made between DIC's computed orbital structures and the referenced charge-distribution charts that were obtained from experimental data.

Analysis of the orbital structure of DIC reveals that it is constructed of four benzene rings that are attached to a central, "isolated" double bond. Analogous double-bond moieties exist in fullerenes, rationalizing the nucleophilic addition reactions that fullerenes undergo. Therefore, while corannulene is considered a good model for $C_{60}$'s magnetic and aromatic properties, DIC emerges as a model for the reactivity features of fullerenes.

## Experimental Section

**Materials.** THF-$d_8$ (Deutero GmbH) was dried over sodium−potassium alloy under vacuum. Lithium (Aldrich) was kept in paraffin oil and was rinsed shortly before use with petroleum ether (bp 40−60 °C). DIC **2a** and **2b** were synthesized as previously reported.[2]

**NMR Spectroscopy.** NMR experiments were carried out using a Bruker DRX-400 spectrometer equipped with a BGUII *z*-gradient, operating at 400.13, 100.62, and 155.51 MHz for $^1$H, $^{13}$C, and $^7$Li NMR, respectively. Due to the low solubility of **2a** in THF, some of the spectroscopic data of the neutral **2a** were recorded in a hot nitrobenzene-$d_5$ solution, and the reported chemical shifts were calibrated to the downfield nitrobenzene signal ($\delta_H$ 8.124 at 298 K; $\delta_C$ 149.64 at 448 K). All other samples were dissolved in THF-$d_8$, and the reported chemical shifts were calibrated to the downfield THF signal ($\delta_H$ 3.575; $\delta_C$ 67.393). The $^7$Li NMR standard was LiCl/D$_2$O at 298 K. A complete NMR assignment was obtained by applying standard two-dimensional NMR techniques such as COSY, NOESY, CH-Correlation, and long-range CH-Correlation along with the use of the carbon-edited NOESY technique[12] as described in the text.

Carbon-edited NOESY is a combination of a regular NOESY and a carbon-edited spectrum. During the acquisition (*t*2), only the proton signals that are coupled to carbon are recorded. These signals are then carbon decoupled in *f*2, leaving the carbon coupling in *f*1. The result is that the carbon satellites that are excited in *f*1 are again active in *f*2 and yield a "double-diagonal" split in *f*1 by the $^1$H, $^{13}$C coupling constant (~158 Hz for PAHs). A signal arising from a proton attached to a

---

[16] Biedermann, P. U.; Pogodin, S.; Agranat, I. *J. Org. Chem.* **1999**, *64*, 3655−3662.

[17] The twisting from planarity in the calculated transition state of DIC$^{4-}$ at the B3LYP/6-311G** level is caused by an overestimation of the proton overcrowding in the bays at this level of calculation, probably due to the inclusion of polarization functions for the hydrogen atoms in the basis set. The planar ($D_{2h}$) structure of DIC$^{4-}$ at the B3LYP/6-311G** level is a saddle point of second order, which is higher in energy than the twisted $D_2$ structure by <0.01 kcal/mol.

[18] As shown in ref 16 for neutral DIC (**2a**), it is found that also in the reduced species the B3LYP calculation with the 6-31G* basis set underestimates the energy barriers for the bowl-to-bowl inversion by >2 kcal/mol (compared to calculations using the 6-311G** basis set).

[19] Seiders, T. J.; Baldridge, K. K.; Grube, G. H.; Siegel, J. S. *J. Am. Chem. Soc.* **2001**, *123*, 517−525.

$^{12}$C that has a NOESY correlation with an identical proton attached to a $^{13}$C will appear on the "true" diagonal, half-way between the "double-diagonal" signals.[12]

**Computational Details.** All computations described herein were carried out using the GAUSSIAN '98 program package[20] with the exception of NBO[14,21] analyses, which employed JAGUAR 4.0 software (Schrödinger, Inc., Portland, OR, 1998).

Most of the calculations were carried out at the DFT level of calculation, employing Becke's three-parameter hybrid density functional with the nonlocal correlation functional of Lee, Yang, and Parr (B3LYP)[22] and the 6-311G** basis set.[23] Energy barriers for bowl-to-bowl inversion were also calculated with Barone and Adamo's Becke-style one-parameter functional using a modified Perdew–Wang exchange and a Perdew–Wang 91 correlation[24] (*m*PW1PW, which is found to be better than B3LYP in estimating the activation energy for the Walden inversion[25]). A Hartree–Fock ab initio calculation was also performed, employing also 3-21G and 6-31G* basis sets (see Table 2). For the graphic depiction of the MO orbitals and NBO calculations, the 6-31G* basis set was used.

All structures that were calculated were geometrically optimized within their symmetry point groups. Only minimum structures were considered for NMR calculations. Planar structures,[17] calculated to estimate the bowl-to-bowl inversion barriers, have been optimized and found to be saddle points of the first order. NMR chemical shifts were derived from additional single-point calculations employing the GIAO[26] method as implemented in GAUSSIAN '98. The isotropy values that were obtained in this way were subtracted from the isotropy values that were obtained for the optimized TMS (B3LYP/6-311G**//B3LYP/6-311G** level: H 32.00 ppm; C 184.44 ppm).

Although we are aware of the importance of the use of diffuse functions in the basis set when calculating anions to reduce the overestimated mutual electron repulsion,[27] we refrained from using a basis set higher than 6-311G** for the following reasons. (a) Diffuse functions are important in the calculation of *atomic* anions[28] and of anionic systems in which the charge is concentrated on individual atoms.[29] However, DIC is a highly conjugated molecule; therefore, the charge in DIC is efficiently *delocalized*, and hence the use of diffuse functions is not mandatory. (b) The main influence of the diffuse functions is on energy calculations rather than on geometrical and electronic structures.[30] The good correlation between the calculated and experimental NMR values, a property that is quite sensitive to geometry changes, supports this approximation. Since we regarded the energy results (the bowl-to-bowl inversion barriers) only qualitatively,[31] it is reasonable to assume that the trend that is shown remains the same even when diffuse functions are included. (c) Finally, the size of the system under investigation along with the restriction of computational resources makes the calculations applying basis sets that include diffuse functions impractical, in particular for the computation of the dimeric systems.

**General Procedure for the Reduction Process.** A lithium wire was freshly produced and directly inserted into the upper part of an extended NMR tube, which was previously filled with argon and contained the material (ca. 5 mg). Dry THF-$d_8$ (ca. 0.5 mL) was vacuum-transferred from a reservoir to the tube. The sample was degassed under vacuum using the freeze–pump–thaw technique and flame-sealed. The solution was brought into contact with the lithium wire by turning the tube upside down.

**Quenching of the Anions.** After completing the analyses on the samples of DIC and **2b** at their tetraanionic states, we quenched the samples with oxygen. The quenching experiments were carried out by opening the samples under anhydrous conditions and blowing the gas via a syringe into the tube. The deep color gradually disappeared, and the $^{1}$H NMR spectra were recorded.

**Diindeno[1,2,3,4-*defg*;1′,2′,3′,4′-*mnop*]chrysene (2a):** $^{1}$H NMR (nitrobenzene-$d_5$, 298 K) $\delta$ 7.69 (H-2, t, $J = 7.6$ Hz, 4 H), 7.96 (H-1, d, $J = 7.1$ Hz, 4 H), 8.30 (H-3, d, $J = 8.1$ Hz, 4 H); $^{1}$H NMR (THF-$d_8$, 298 K) $\delta$ 7.63 (H-2, dd, $J = 7.6$, 7.1 Hz, 4 H), 7.94 (H-1, d, $J = 7.3$ Hz, 4 H), 8.34 (H-3, d, $J = 8.0$ Hz, 4 H); $^{13}$C NMR (nitrobenzene-$d_5$, 448 K) $\delta$ 123.16 (C-1), 125.21 (C-3), 129.62 (C-2), 134.15 (C-3a), 137.31 (C-12d), 139.32 (C-6c), 142.38 (C-6a).

**Dianion ($2a^{2-}/2Li^{+}$):** $^{1}$H NMR (THF-$d_8$, 230 K) $\delta$ 5.70 (H-3, d, $J = 4.0$ Hz, 4 H), 5.70 (H-1, d, $J = 4.0$ Hz, 4 H), 6.70 (H-2, t, $J = 4.0$ Hz, 4 H); $^{13}$C NMR (THF-$d_8$, 230 K) $\delta$ 104.17 (C-12d), 112.34 (C-3), 114.95 (C-1), 122.70 (C-2), 126.43 (C-6a), 136.01 (C-3a), 146.06 (C-6c); $^{7}$Li NMR (THF-$d_8$, 230 K) $\delta$ −0.4.

**Tetraanion ($2a^{4-}/4Li^{+}$):** $^{1}$H NMR (THF-$d_8$, 165 K) $\delta$ 4.28 (H-3, s, 4 H), 4.89 (H-1, s, 4 H), 5.46 (H-2, s, 4 H); $^{13}$C NMR (THF-$d_8$, 165 K) $\delta$ 85.6 (C-3), 96.6 (C-1), 103.1 (C-12d), 117.4 (C-6a), 120.7 (C-2), 127.7 (C-3a), 139.3 (C-6c); $^{7}$Li NMR (THF-$d_8$, 160 K) $\delta$ −6.2, −4.9, −1.8 (band of peaks), 0.2, 0.6, 0.8, 1.2, 1.5, 1.9. $^{7}$Li NMR spectrum was temperature dependent. At high temperatures, only the peaks at positive $\delta$ values appear.

**2,5,8,11-Tetra-*tert*-butyldiindeno[1,2,3,4-*defg*;1′,2′,3′,4′-*mnop*]chrysene (2b):** $^{1}$H NMR (THF-$d_8$, 298 K) $\delta$ 1.50 (Me, s, 36 H), 8.05 (H-1, s, 4 H), 8.34 (H-3, s, 4 H); $^{13}$C NMR (THF-$d_8$, 298 K) $\delta$ 32.40 (Me), 36.73 ($^{t}$Bu), 120.84 (C-1), 121.00 (C-

---

[20] Frisch, M. J.; Trucks, G. W.; Schlegel, H. B.; Scuseria, G. E.; Robb, M. A.; Cheeseman, J. R.; Zakrzewski, V. G.; Montgomery, J. A., Jr.; Stratmann, R. E.; Burant, J. C.; Dapprich, S.; Millam, J. M.; Daniels, A. D.; Kudin, K. N.; Strain, M. C.; Farkas, O.; Tomasi, J.; Barone, V.; Cossi, M.; Cammi, R.; Mennucci, B.; Pomelli, C.; Adamo, C.; Clifford, S.; Ochterski, J.; Petersson, G. A.; Ayala, P. Y.; Cui, Q.; Morokuma, K.; Malick, D. K.; Rabuck, A. D.; Raghavachari, K.; Foresman, J. B.; Cioslowski, J.; Ortiz, J. V.; Stefanov, B. B.; Liu, G.; Liashenko, A.; Piskorz, P.; Komaromi, I.; Gomperts, R.; Martin, R. L.; Fox, D. J.; Keith, T.; Al-Laham, M. A.; Peng, C. Y.; Nanayakkara, A.; Gonzalez, C.; Challacombe, M.; Gill, P. M. W.; Johnson, B. G.; Chen, W.; Wong, M. W.; Andres, J. L.; Head-Gordon, M.; Replogle, E. S.; Pople, J. A. *Gaussian 98*, revision A.7; Gaussian, Inc.: Pittsburgh, PA, 1998.

[21] Glendening, E. D.; Badenhoop, J. K.; Reed, A. D.; Carpenter, J. E.; Weinhold, F. *NBO 4.M.*; Theoretical Chemistry Institute, University of Wisconsin: Madison, WI, 1999.

[22] (a) Becke, A. D. *J. Chem. Phys.* **1993**, *98*, 5648–5652. (b) Lee, C.; Yang, W.; Parr, R. G. *Phys. Rev. B* **1988**, *37*, 785–789. (c) Miehlich, B.; Savin, A.; Stoll, H.; Preuss, H. *Chem. Phys. Lett.* **1989**, *157*, 200–206.

[23] (a) Hehre, W. J.; Ditchfield, R.; Pople, J. A. *J. Chem. Phys.* **1972**, *56*, 2257–2261. (b) Hariharan, P. C.; Pople, J. A. *Theor. Chim. Acta* **1973**, *28*, 213–222. (c) Krishnan, R.; Binkley, J. S.; Seeger, R.; Pople, J. A. *J. Chem. Phys.* **1980**, *72*, 650–654.

[24] Adamo, C.; Barone, V. *Chem. Phys. Lett.* **1997**, *274*, 242–250.

[25] Adamo, C.; Barone, V. *J. Chem. Phys.* **1998**, *108*, 664–675.

[26] Wolinski, K.; Hilton, J. F.; Pulay, P. *J. Am. Chem. Soc.* **1990**, *112*, 8251–8260.

[27] Clark, T.; Chandrasekhar, J.; Spitznagel, G. W.; Schleyer, P. v. R. *J. Comput. Chem.* **1983**, *4*, 294–301.

[28] Diffuse functions are essential to reproduce the negative orbital energies of the highest occupied orbitals of atomic negative anions. See, for example: (a) Jareci, A. A.; Davidson, E. R. *Chem. Phys. Lett.* **1999**, *300*, 44–52; (b) Galbraith, J. M.; Schaefer, H. F., III. *J. Chem. Phys.* **1996**, *105*, 862–864.

[29] (a) Driessler, F.; Ahlrichs, R.; Staemmler, V.; Kutzelnigg, W. *Theor. Chim. Acta* **1973**, *30*, 315–326. (b) Duke, A. J. *Chem. Phys. Lett.* **1973**, *21*, 275–282.

[30] DFT calculations on the pentalene dianion (modeling a simple, delocalized anion), comparing basis sets including/omitting diffuse functions, show that the geometry predicted by both basis sets is practically the same, and NMR values and partial charges also agree within >99% correlation (to be published).

[31] In principle, using *any* finite basis set in the calculations of high anions, which are thought to be unbound in the gas phase, forces the electrons to remain attached to the molecular skeleton. Therefore, the ground-state energy evaluation is only an approximation, including diffuse functions or not, and thus the energy results can only be regarded qualitatively. The conventional assumption is that the calculated electronic and geometrical structures are not too different from the structures in solution. See: (a) Green, W. H., Jr.; Gorun, S. M.; Fitzgerald, G.; Fowler, P. W.; Ceulemans, A.; Titeca, B. C. *J. Phys. Chem.* **1996**, *100*, 14892–14898. (b) Negri, F.; Orlandi, G.; Zerbetto, F. *Chem. Phys. Lett.* **1988**, *144*, 31–37. We are currently investigating the many faces of the calculations of charged polycyclic aromatic hydrocarbons, addressing especially the question of the necessity of including diffuse functions in the basis sets in the calculations of anions conjugated in such an extended manner.[30]

3), 134.51 (C-3a), 138.68 (C-12d), 139.19 (C-6c), 142.36 (C-6a), 153.29 (C-2).

**Dianion ($2b^{2-}/2Li^{+}$):** $^1$H NMR (THF-$d_8$, 220 K) $\delta$ 1.19 (Me, s, 36 H), 5.93 (H-3, s, 4 H), 6.78 (H-1, s, 4 H); $^{13}$C NMR (THF-$d_8$, 220 K) $\delta$ 33.17 (Me), 35.12 ($^t$Bu), 104.06 (C-12d), 110.39 (C-3), 118.31 (C-1), 124.90 (C-6a), 135.54 (C-3a), 135.72 (C-2), 145.21 (C-6c); $^7$Li NMR (THF-$d_8$, 220 K) $\delta$ −0.2.

**Tetraanion ($2b^{4-}/4Li^{+}$):** $^1$H NMR (THF-$d_8$, 165 K) $\delta$ 1.14 (Me, s, 36 H), 4.49 (H-3, s, 4 H), 4.95 (H-1, s, 4 H); $^{13}$C NMR (THF-$d_8$, 165 K) $\delta$ 33.21 (Me), 35.34 ($^t$Bu), 84.10 (C-3), 93.21 (C-1), 101.28 (C-12d), 118.17 (C-6a), 126.44 (C-3a), 138.58 (C-6c), 140.59 (C-2); $^7$Li NMR (THF-$d_8$, 165 K) $\delta$ −7.2, −4.2, −2.4, a broad band ranging from 0 to 2. The $^7$Li NMR spectrum was temperature dependent. At high temperatures, only the broad band at positive $\delta$ values appears.

**Acknowledgment.** Financial support from the U.S.−Israel Binational Science Foundation (BSF), Lise Meitner-Minerva Center for Computational Quantum Chemistry, and U.S. National Science Foundation is gratefully acknowledged. R.S. is also indebted to Prof. Sason Shaik, Prof. Klaus Müllen, and Prof. Gernot Frenking for very fruitful discussions, and to Dr. David Danovich for the support in the computations. R.B. thanks the Minerva Foundation for a postdoctoral fellowship.

**Supporting Information Available:** Carbon-edited NOESY spectra of **2b** and **2b**$^{2-}$, $^7$Li NMR spectra of **2a**$^{4-}$ at various temperatures, and Cartesian coordinates and computed total energies of all calculated species mentioned in Table 2. This material is available free of charge via the Internet at http://pubs.acs.org.

JO010103F